ACS APPLIED MATERIALS & INTERFACES

Research Article

www.acsami.org

Synthesis of Magnetically Separable $Ag_3PO_4/TiO_2/Fe_3O_4$ Heterostructure with Enhanced Photocatalytic Performance under Visible Light for Photoinactivation of Bacteria

Jing-Wen Xu,[†,‡] Zhi-Da Gao,[†,‡] Kun Han,[†] Yongmin Liu,[§] and Yan-Yan Song*[,†]

[†]College of Sciences, Northeastern University, Shenyang 110004, China

[§]Department of Mechanical & Industrial Engineering, Department of Electrical & Computer Engineering, Northeastern University, Boston, Massachusetts 02115, United States

Supporting Information

ABSTRACT: Silver orthophosphate (Ag_3PO_4) is a low-band-gap photocatalyst that has received considerable research interest in recent years. In this work, the magnetic $Ag_3PO_4/TiO_2/Fe_3O_4$ heterostructured nanocomposite was synthesized. The nanocomposite was found to exhibit markedly enhanced photocatalytic activity, cycling stability, and long-term durability in the photodegradation of acid orange 7 (AO7) under visible light. Moreover, the antibacterial film prepared from $Ag_3PO_4/TiO_2/Fe_3O_4$ nanocomposite presented excellent bactericidal activity and recyclability toward *Escherichia coli* (*E. coli*) cells under visible-light irradiation. In addition to the intrinsic cytotoxicity of silver ions, the elevated bactericidal efficiency of $Ag_3PO_4/TiO_2/Fe_3O_4$ can be largely attributed to its highly enhanced photocatalytic activity. The photogenerated hydroxyl radicals and superoxide ions on the formed $Ag/Ag_3PO_4/TiO_2$ interfaces cause considerable morphological changes in the microorganism's cells and lead to the death of the bacteria.

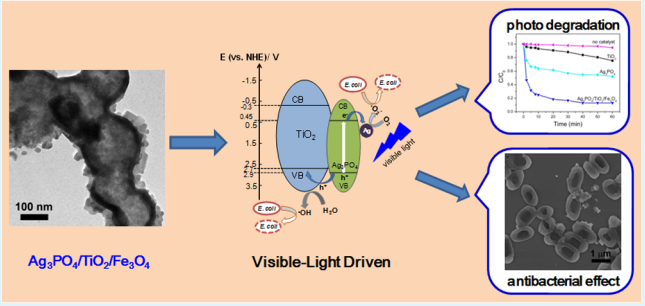

KEYWORDS: *photocatalyst, heterostructure, visible light, photoinactivation, bactericidal activity, recyclability*

1. INTRODUCTION

Photocatalysts, such as TiO_2,[1,2] ZnO,[3] and Mo_2O_3,[4] can be used as antimicrobial materials in the killing or growth inhibition of bacteria. As one well-known component, titanium dioxide (TiO_2) has been extensively studied since Fujishima and Honda demonstated its high photocatalytic activity.[5] TiO_2 shows great prospects as a photocatalyst in decomposing organic pollutants in the environment, as a self-cleaning coating for buildings, and also as an antimicrobial material.[6−10] When TiO_2 is irradiated with light with an energy equal to or greater than its band-gap energy, electron−hole pairs are generated in the photocatalyst and subsequently react with H_2O and O_2 molecules to produce highly reactive hydroxyl radicals and superoxide ions, respectively, at the catalyst/water interface. The resulting active oxygen species can oxidize and damage the cells of microorganisms at the surface of the catalyst.[11] However, because of its wide band gap ($E_g \approx 3.0-3.2$ eV), TiO_2 is particularly suitable for applications based on UV-light irradiation. Additionally, the practical application of TiO_2 is also limited by its insufficient electron−hole separation, which leads to a lower energy conversion.[12]

Very recently, a breakthrough was made by Yi et al., who reported the use of silver orthophosphate (Ag_3PO_4) to oxidize water and decompose organic contaminants in aqueous solutions by visible-light irradiation.[13] Ag_3PO_4 has a relatively narrow band gap (2.36−2.43 eV) and is thus active under visible-light irradiation (λ < 530 nm). Therefore, as a highly efficient photocatalyst, Ag_3PO_4 could behave as a potential antimicrobial material and could have promise in various antimicrobial applications.[14,15] Furthermore, silver and silver-based compounds are well-known antimicrobial biomaterials because of their low toxicity for mammalian cells and excellent broad-spectrum antimicrobial activity.[16−21] However, Ag_3PO_4 is prone to photoreduction and decomposition if no sacrificial reagent is supplied.[22,23] To overcome this problem, many studies have focused on heterocoupling,[24,25] fabricating signal crystals,[26] decreasing the particle size,[27] and synthesizing Ag/Ag_3PO_4 plasmonic nanocomposites.[28,29] As the valence band (VB) level of Ag_3PO_4 is located lower than that of TiO_2, holes that are photogenerated in Ag_3PO_4 can transfer to TiO_2, and these energetic holes in the VB of TiO_2 are, in turn, able to initiate various oxidation reactions. Therefore, combining Ag_3PO_4 with TiO_2 to form hetrostructures is regarded as an effective strategy for achieving efficient photocatalysts with high photocatalytic activities under visible-light irradiation.[22−25] Moreover, Teng et al. found that the silver (Ag^0) nanoparticles formed on the

Received: May 25, 2014
Accepted: August 20, 2014
Published: August 20, 2014

surface of Ag_3PO_4 can act as electron acceptors to enhance the charge separation and prevent the reductive decomposition of Ag_3PO_4.[29] At the same time, the effect of the surface plasmon resonance of metallic silver can further increase the absorption of visible light. Nevertheless, despite its well-known photocatalytic activity under visible light, still very few research groups have attempted to employ Ag_3PO_4 as an antibacterial material by the photoinactivation process.[14,15,30] Moreover, in practical application, it is relatively difficult to isolate and recover nanosized photocatalysts from a mixed suspension after a photocatalytic reaction to avoid secondary contamination. Magnetic photocatalysts represent an alternative for addressing this problem.[31,32] These photocatalysts can be easily recovered by a magnet and can be recovered from a photocatalysis reaction system several times without any appreciable reduction in photocatalytic efficiency.

To the best of our knowledge, until now, no report has been focused on the preparation of magnetic $Ag_3PO_4/TiO_2/Fe_3O_4$ nanocomposite and the exploration of its antibacterial activity, even though the photocatalytic activities of Ag_3PO_4 and its hierarchical nanostructures are widely recognized and have triggered extensive research interest. The aim of the present work was to develop a magnetically recoverable photocatalyst with excellent photoinactivation properties toward bacteria under visible-light irradiation. Detailed investigations of the photocatalytic activity of $Ag_3PO_4/TiO_2/Fe_3O_4$ nanoparticles and their photoinactivation toward *E. coli* were carried out under visible-light irradiation. Compared to TiO_2 and Ag_3PO_4, the as-formed $Ag_3PO_4/TiO_2/Fe_3O_4$ nanocomposite was found to exhibit highly improved excellent performances in antimicrobial applications.

2. EXPERIMENTAL SECTION

2.1. Materials and Reagents. $FeCl_3{\cdot}6H_2O$, $FeCl_2{\cdot}3H_2O$, $AgNO_3$, Na_2HPO_4, $Ti(SO_4)_2$, and poly(ethylene glycol) (PEG-600) were purchased from Sigma-Aldrich Chemicals Co. $NH_3{\cdot}H_2O$, urea, tetrabutyl titanate, and other chemicals were purchased from Sinopharm Chemical Reagent Co. Ltd. and used without further purification. All aqueous solutions were prepared with deionized (DI) water (>18 MΩ).

2.2. Preparation of $Ag_3PO_4/TiO_2/Fe_3O_4$ Nanospheres. To prepare Fe_3O_4 nanoparticles, 5.4 g of $FeCl_3{\cdot}6H_2O$ and 2.0 g of $FeCl_2{\cdot}4H_2O$ were dissolved in 25.0 mL of HCl (2.0 M) with degassing of the solution by nitrogen (N_2) gas. Then, 30.0 mL of ammonia (NH_3) solution [25% (v/v)] was added to the mixture, which was then stirred vigorously for 30 min. N_2 gas was passed continuously through the mixture during the reaction. The black product was collected with an external magnet, rinsed three times with distilled water, and then resuspended in deionized water.

TiO_2-capped Fe_3O_4 nanoparticles were prepard by in situ hydrolysis. In a typical process, 1.25 mL of Fe_3O_4 suspension (6 mg/mL) was dispersed in 22.75 mL of DI water. Then, 0.55 mL of $Ti(SO_4)_2$ (0.5 M) was added under stirring. After the resulting solution had been heated to 80 °C, 0.5 mL of urea solution (0.5 M) and 0.8 mL of PEG-600 solution (0.048 M) were added with constant stirring. The mixture was then refluxed at 80 °C for 1 h. The product was separated by an external magnet; washed with ethanol and distilled water, three times each; and finally dried at 60 °C in a vacuum oven. The dried powders were annealed in Ar at 360 °C for 6 h.

The deposition of Ag_3PO_4 nanoparticles onto the TiO_2/Fe_3O_4 surface was carried out by the precipitation method. Briefly, 5.0 mg of TiO_2/Fe_3O_4 power was dispersed in 20.0 mL of DI water; then 1.0 mL of Na_2HPO_4 (0.15 M) was added, and the solution was sonicated for 2 h. Subsequently, 3.0 mL of $AgNO_3$ solution (0.15 M) was dropped into this solution. The resulting nanocomposites were redispersed in 20.0 mL of DI water and then sealed in a Teflon-lined stainless steel autoclave for hydrothermal treatment at 160 °C for another 2 h.

2.3. Photocatalytic Tests. To evaluate the photocatalytic activities of the photocatalysts, the performance of as-formed photocatalyst was evaluated in the degradation of azo dye acid orange 7 (AO7, $C_{16}H_{12}N_2O_4S$) in water. In a typical photocatalytic reaction, an amount of photocatalyst was added to a solution of AO7 (15 μM, 3.0 mL), and the mixture was kept in the dark for 30 min under continuous stirring to achieve the equilibrium adsorption of AO7 on the photocatalyst surface. Photocatalytic degradation was carried out by illuminating the suspension with visible light (ca. 0.8 cm^2) using a 50-mW diode blue laser (λ = 405 nm). All photocatalytic experiments were carried out at room temperature under continuous stirring. The degradation of AO7 was monitored by UV−vis spectroscopy at different time intervals. To test the recyclability of the catalyst, the $Ag_3PO_4/TiO_2/Fe_3O_4$, nanoparticles were separated with an external magnet after AO7 had been completely decomposed and washed under flowing DI water three times before the next photocatalytic reaction.

2.4. Preparation of Photocatalyst-Containing Antibacterial Films. In general, suspensions of the as-prepared photocatalyst nanoparticles (0.3 mg) were dripped onto filter paper (Φ 15 mm) separately. After being allowed to dry in air, the filter papers were then placed onto the bottom of a Petri dish for antibacterial experiments. Control samples were prepared by using filter paper without loading any nanoparticles. After the antibacterial tests, the films were washed with phosphate-buffered saline (PBS, 10 mM, pH 7.0) to remove the entrapped bacterial bodies . The films were then dried and stored at room temperature.

2.5. Antibacterial Tests. Antibacterial activities were evaluated using Gram-negative DH5α *Escherichia coli* (*E. coli*). The bacterial suspensions employed for the test contained 10^7 colony-forming units per milliliter (CFU mL^{-1}). Before the microbiological experiments, all glasswares was sterilized by autoclaving at 120 °C for 30 min. For each antibacterial experiment, the prepared photocatalyst-containing antibacterial film was placed onto the bottom of a Petri dish containing 10 mL of *E. coli* suspension. Then, the antibacterial experiment was initiated by irradiating the suspension with a commercial 300-W xenon lamp equipped with a UV cutoff filter (λ > 420 nm). The light source was located 20 cm from the reaction solution (50 mW cm^{-2} illumination intensity). After irradiation, 1 mL of the treated bacterial suspension was withdrawn and diluted serially with sterilized Milli-Q water to adjust the bacterial concentration (aliquots were diluted to 10^{-5} times in the present study) to ensure that the growing bacterial colonies were being counted accurately and easily. To quantify the antimicrobial results, 100 μL of the treated solution was spread on a lysogeny broth (LB) agar plate (LB liquid medium with 1.5% agar), and the colonies were counted to determine the survival bacterial numbers after incubation at 37 °C for 24 h. The bactericidal efficiency of the photocatalyst-containing film was determined by comparing the corresponding colony counts with those obtained for control films (prepared in the dark without addition of nanoparticles), according to the equation[33]

$$\text{bactericidal efficiency (\%)} = \frac{N_{\text{control}} - N_{\text{sample}}}{N_{\text{control}}} \times 100\% \quad (1)$$

where N_{control} and N_{sample} correspond to the numbers of colonies counted in the control and sample agar plates, respectively.

2.6. Disk Diffusion Assays. *E. coli* suspension (10^7 CFU/mL) was spread on the surface of LB plates. Sterilized Oxford cups (Φ 6 mm) were then placed on the plates and filled with 0.1 mg of photocatalyst. After exposure to visible light for 5 min, the plates were incubated at 37 °C for 24 h. All tests were performed in triplicate, and the results were averaged.

2.7. Detection of •OH Radicals. Terephthalic acid (TA) was used without further purification. An aqueous solution containing 0.01 M NaOH, 0.1 M KCl, 0.3 mM H_2O_2, and 3 mM TA was prepared, and then 0.3 mg of Ag_3PO_4 or $Ag_3PO_4/TiO_2/Fe_3O_4$ powder was suspended in 3.5 mL of this solution in a 1 cm × 1 cm quartz cuvette. The sample cell was placed on a magnetic stirrer and irradiated under a diode blue laser (λ = 405 nm) for 0−90 min. Fluorescence spectra of the supernatant liquid were measured with a fluorescence spectrophotometer (Hitachi F-7000).

2.8. Apparatus. The morphologies of the nanoparticles and bacteria were characterized by field-emission scanning electron microscopy (FE-SEM; Hitachi S-4800, Tokyo, Japan) and transmission electron microscopy (TEM; JEOL 2000). X-ray diffraction (XRD) patterns were acquired on an X'Pert X-ray diffraction spectrometer (Philips, Guildford, Surrey, U.K.) with a Cu Kα X-ray source. UV−vis absorption spectra were measured on a spectrophotometer (Perkin-Elmer, Lambda XLS+, Wellesley, MA). The size of the nanoparticles was analyzed on a Zetasizer Nano ZS90 instrument (Malvern Instruments, Malvern, U.K.). X-ray photoelectron spectroscopy (XPS) was performed on a Perkin-Elmer Physical Electronics 5600 spectrometer using Al Ka radiation at 13 kV as the excitation source. The takeoff angle of the emitted photoelectrons was 45°, with a resolution of 0.1 eV. Inductively couple plasma mass spectrometry (ICP-MS; Agilent 7500) was used for the quantification of leached silver ions. Fluorescence emission spectra were recorded on a Hitachi F-7000 type fluorescence spectrometer.

3. RESULTS AND DISCUSSION

3.1. Structural Characterization of As-Prepared Photocatalysts. The mean diameter of the Fe_3O_4 nanoparticles was ~10 nm (Figure S1, Supporting Information). After a layer of TiO_2 was wrapped around the Fe_3O_4 surface, the diameter of TiO_2/Fe_3O_4 increased to 100 ± 30 nm (denoted as TiO_2/Fe_3O_4, Figure S2, Supporting Information). Because of the magnetism of Fe_3O_4, some agglomerations of TiO_2/Fe_3O_4 nanoparticles appeared. In Figure 1, the morphology of the as-prepared

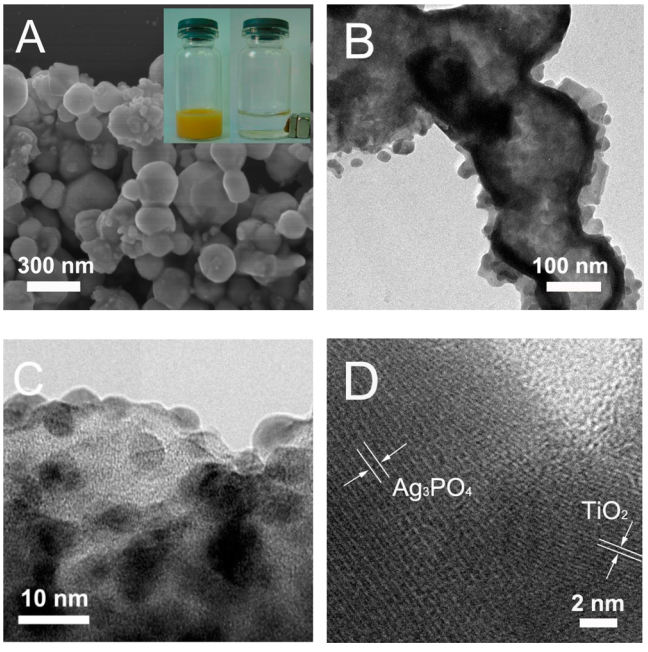

Figure 1. (A) SEM and (B) TEM images of the as-synthesized $Ag_3PO_4/TiO_2/Fe_3O_4$ nanospheres. (C) HRTEM images of Ag_3PO_4 particles on the $Ag_3PO_4/TiO_2/Fe_3O_4$ nanospheres. (D) Spacing of TiO_2 and Ag_3PO_4 lattice fringes. Inset in panel A: Photographs of $Ag_3PO_4/TiO_2/Fe_3O_4$, which were easily dispersed in water (left) and drawn from the solution to the sidewall of the vial by an external magnet (right).

$Ag_3PO_4/TiO_2/Fe_3O_4$ composites was investigated by field-emission scanning electron microscopy (FE-SEM) and transmission electron microscopy (TEM). It can be seen that the diameter of the synthesized $Ag_3PO_4/TiO_2/Fe_3O_4$ hierarchical nanoparticles was about 200 ± 50 nm after Ag_3PO_4 had been loaded. The as-formed $Ag_3PO_4/TiO_2/Fe_3O_4$ nanoparticles were well-dispersed in water, and the suspended nanoparticles could be easily drawn to the side wall of the vial with a magnet (inset of Figure 1A), implying good magnet-controlled properties and recyclability. The decorated Ag_3PO_4 nanoparticles could also be distinguished on the hierarchical nanostructure by high-resolution TEM (HRTEM, Figure 1C) with sizes ranging from 5 to 10 nm. These Ag_3PO_4 nanoparticles were in intimate contact with the TiO_2 support, and the lattice fringes of both Ag_3PO_4 and TiO_2 can be clearly identified in Figure 1D. The lattice constant of about 0.65 nm is consistent with the body-centered-cubic (bcc) structure of Ag_3PO_4,[31,34,35] and the lattice spacing of 0.35 nm is in agreement with the spacing of anatase TiO_2(101) lattice planes (ICDD-JCPDS database, 21-1272). Furthermore, the distribution of each element in $Ag_3PO_4/TiO_2/Fe_3O_4$ was examined by high-angle annular dark-field scanning transmission electron microscopy (HAADF-STEM) and energy-dispersive X-ray spectroscopy (EDS) measurements. The results are shown in Figure S4 (Supporting Information). As manifested by the cross-sectional compositional line profile, Ag was found throughout the whole nanoparticle with very high intensity, whereas Fe and Ti were detected only near the center region, at a lower intensity.

X-ray diffraction (XRD) patterns of Ag_3PO_4, TiO_2/Fe_3O_4, and $Ag_3PO_4/TiO_2/Fe_3O_4$ are presented in Figure 2A. The Ag_3PO_4 nanoparticles exhibited a bcc structure. The diffraction peaks

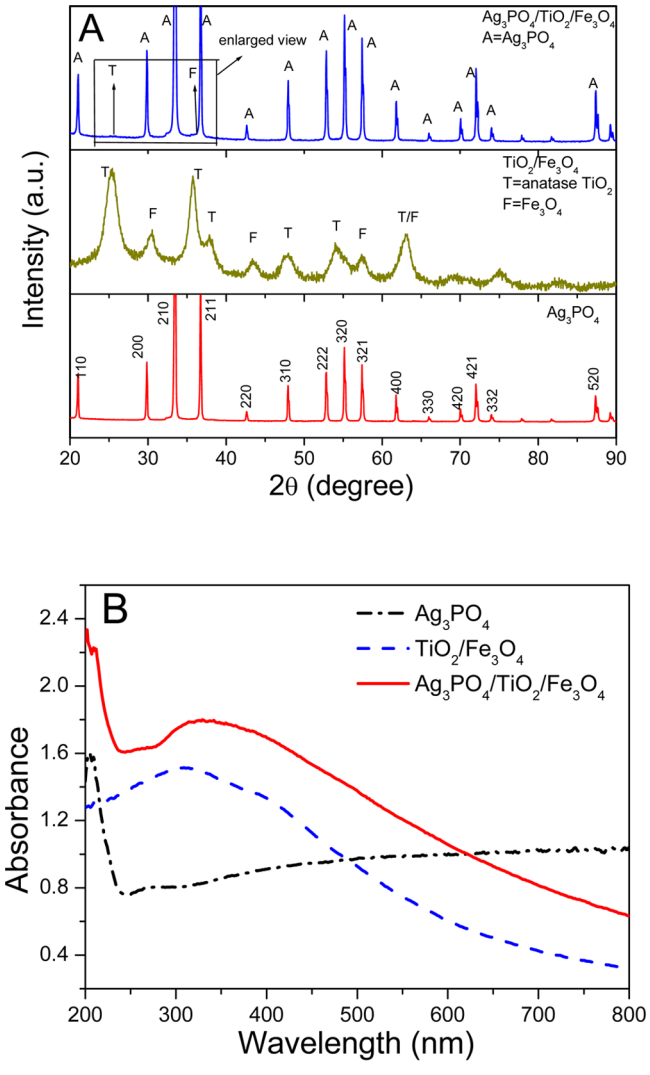

Figure 2. (A) XRD patterns and (B) UV−vis absorption spectra of Ag_3PO_4, TiO_2/Fe_3O_4, and $Ag_3PO_4/TiO_2/Fe_3O_4$ nanoparticles.

dx.doi.org/10.1021/am5032727 | ACS Appl. Mater. Interfaces 2014, 6, 15122−15131

corresponding to Ag_3PO_4 were also present for $Ag_3PO_4/TiO_2/Fe_3O_4$ nanocomposite. Meanwhile, the anatase diffraction peaks of TiO_2 and the diffraction peaks of Fe_3O_4 could also be distinguished in the XRD pattern of $Ag_3PO_4/TiO_2/Fe_3O_4$ (enlarged view in Figure S5, Supporting Information). Figure 2B shows UV−vis absorption spectra of the photocatalyst suspensions. Ag_3PO_4 exhibits an obvious absorption band in the visible-light range (~500 nm). For the $Ag_3PO_4/TiO_2/Fe_3O_4$ nanocomposite, in addition to the absorption band of Ag_3PO_4, the adsorption bands of pure Fe_3O_4 (~370 nm) and TiO_2 (~320 nm) also appeared. Additionally, it is noted that the absorption intensity of the $Ag_3PO_4/TiO_2/Fe_3O_4$ suspension was enhanced in the visible region compared to that of the Ag_3PO_4 suspension, which indicates that the ability of $Ag_3PO_4/TiO_2/Fe_3O_4$ to absorb visible light was much stronger. This property should make a positive contribution to photocatalytic activity, because the more efficient utilization of solar energy could be achieved.[14]

3.2. Photocatalytic Activities of $Ag_3PO_4/TiO_2/Fe_3O_4$ Hierarchical Nanoparticles. Acid orange 7 (AO7, 15 μM), with a major absorption band at 487 nm (Figure S6, Supporting Information), is usually used as a model pollutant for testing the photocatalytic activities of photocatalysts. In this study, the photocatalytic degradation of AO7 was carried out under visible light from a laser at 405 nm without using any sacrificial reagent (setup shown in Figure S7, Supporting Information). The effect of the concentration of $Ag_3PO_4/TiO_2/Fe_3O_4$ on the speed of photocatalytic degradation was investigated first by adding different quantities of $Ag_3PO_4/TiO_2/Fe_3O_4$ nanoparticles to AO7 aqueous solutions. As shown in Figure 3A, AO7 degradation occurred only after the addition of $Ag_3PO_4/TiO_2/Fe_3O_4$ nanoparticles, and the AO7 degradation rate increased with increasing photocatalyst concentration. For example, only ~45% of AO7 was decomposed after 2 min when the $Ag_3PO_4/TiO_2/Fe_3O_4$ suspended concentration was 0.1 mg/mL, but most of the AO7 could be decomposed in 2 min when the photocatalyst concentration reached 0.5 mg/mL. Compared to the results recorded for Ag_3PO_4 (Figure S8, Supporting Information), it is obvious that AO7 photodegraded more rapidly on $Ag_3PO_4/TiO_2/Fe_3O_4$ nanocomposite at the same nanoparticle concentration. Furthermore, it was also noticed that the $Ag_3PO_4/TiO_2/Fe_3O_4$ nanoparticles became dark after the photocatalytic reaction. (The same color change was also observed on the Ag_3PO_4 nanoparticles.) A similar phenomenon was also observed by other groups, who reported that this color change could originate from the formation of Ag^0 species through the reduction of Ag_3PO_4 by photoinduced electrons.[20]

To further investigate the influence of the hierarchical structure on photocatalytic ability, the photocatalytic activity in the degradation of AO7 under visible light was compared using $Ag_3PO_4/TiO_2/Fe_3O_4$, TiO_2, and Ag_3PO_4 nanoparticles as the photocatalysts. (TiO_2 and Ag_3PO_4 nanoparticles were prepared by a similar approach as described in the Experimental Details in the Supporting Information, and the morphologies are characterized in Figure S3 of the Supporting Information.) As displayed in Figure 3B, because of the weak absorption of pure TiO_2 in the visible-light region, TiO_2 nanoparticles showed only a very low photocatalytic activity for AO7 degradation under visible-light irradiation. On the other hand, because of the small band gap of Ag_3PO_4, the utilization of visible light was improved efficiently.[13,36] As expected, the as-formed Ag_3PO_4 and $Ag_3PO_4/TiO_2/Fe_3O_4$ samples showed significantly enhanced photocatalytic activities in the degradation of AO7 under visible light. Moreover, the $Ag_3PO_4/TiO_2/Fe_3O_4$ composites exhibited a much higher photocatalytic activity than the Ag_3PO_4 nanoparticles.

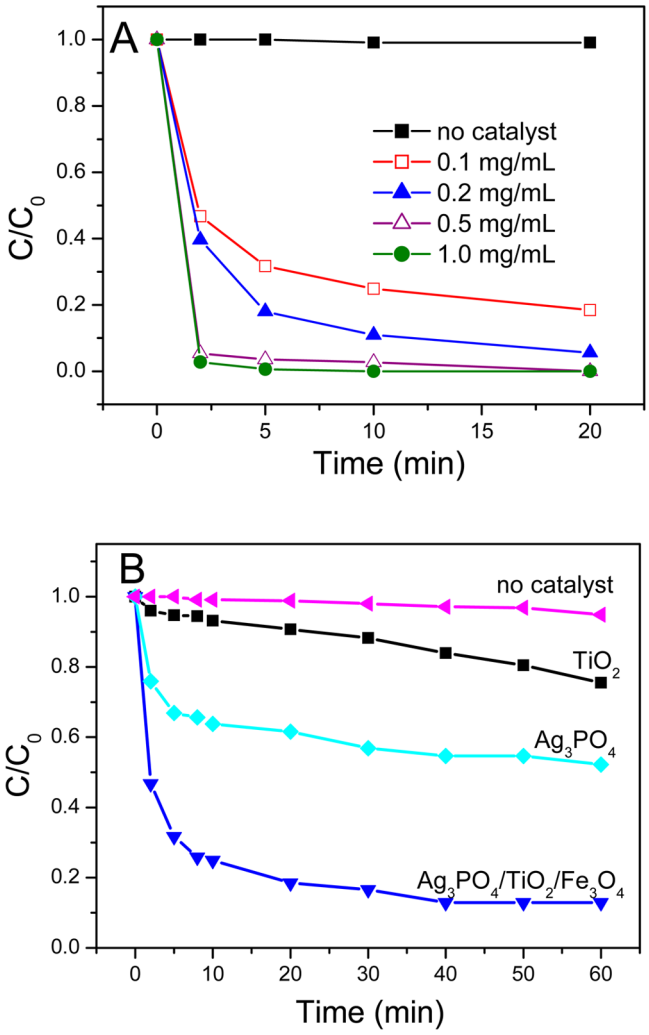

Figure 3. (A) Comparison of photocatalytic degradation of AO7 with different concentrations of $Ag_3PO_4/TiO_2/Fe_3O_4$ under visible-light irradiation. (B) Photocatalytic activities obtained with photocatalysts TiO_2, Ag_3PO_4, and $Ag_3PO_4/TiO_2/Fe_3O_4$ and without photocatalyst for AO7 degradation under visible-light irradiation. The photocatalyst concentration was 0.1 mg/mL.

The stability of a photocatalyst is an important parameter in practical applications. Herein, the activity and stability of $Ag_3PO_4/TiO_2/Fe_3O_4$ were evaluated by examining its recyclability in the photocatalytic degradation of AO7. The photocatalytic stabilities of the catalysts were tested in five successive AO7 degradation experiments using the same $Ag_3PO_4/TiO_2/Fe_3O_4$ sample (1.0 mg/mL). For comparison, the recyclabilities of TiO_2 and Ag_3PO_4 were tested under the same conditions. As plotted in Figure 4, after five photocatalytic experiments, the photodegradation ability of the $Ag_3PO_4/TiO_2/Fe_3O_4$ sample was almost identical to that of the fresh sample. The degraded AO7 decreased from 86% to 67% in five successive experimental runs when using Ag_3PO_4 as the photocatalyst, whereas the degraded AO7 decreased from 48% to 37% when TiO_2 was used as the photocatalyst. The amount of silver ions released from the photocatalysts was also investigated. Figure S9A (Supporting Information) shows a plot of the released silver ion concentration as a function of time. The quantity of silver ion released from the Ag_3PO_4 sample increased sharply in the

dx.doi.org/10.1021/am5032727 | ACS Appl. Mater. Interfaces 2014, 6, 15122−15131

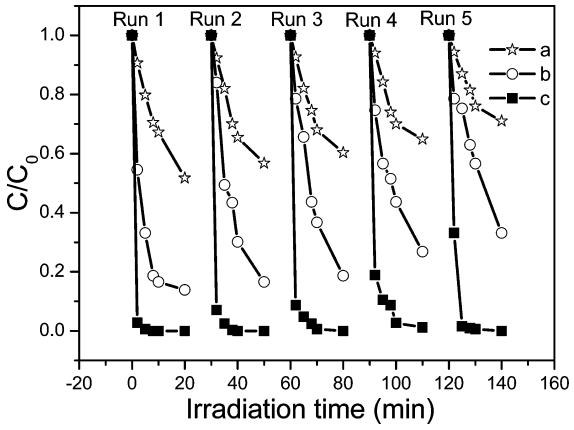

Figure 4. Photocatalytic activities of (a) TiO_2, (b) Ag_3PO_4, and (c) $Ag_3PO_4/TiO_2/Fe_3O_4$ photocatalysts for the degradation of AO7 under visible-light irradiation for five cycles.

beginning, whereas the release of silver ions from $Ag_3PO_4/TiO_2/Fe_3O_4$ was relatively slow. For both photocatalysts, the silver ion concentration was noticed to decrease after 30 min, which can be attributed the reduction of Ag^+ to Ag^0 on the photocatalyst surface by the photogenerated electrons.

3.3. Photocatalytic Antibacterial Characteristics. Concerning the prospective application of $Ag_3PO_4/TiO_2/Fe_3O_4$ under visible-light exposure, the photocatalytic antibacterial properties of the as-synthesized catalyst was investigated in the present work. *Escherichia coli* (*E. coli*), which is responsible for many infections in daily life,[33] served as the model target microorganism. As illustrated in Scheme 1, the bactericidal efficiency against *E. coli* was studied for an antibacterial film, which was prepared by loading the photocatalyst onto filter paper. First, the effects of the presence of photocatalyst and visible light ($\lambda > 400$ nm) were explored. As shown in Figure S10 (Supporting Information), visible-light irradiation alone did not show any significant bactericidal effects on *E. coli* in the absence of photocatalyst. After 0.30 mg of $Ag_3PO_4/TiO_2/Fe_3O_4$ nanoparticles had been loaded, ~42% of *E. coli* cells were inactivated after 50 min even in the dark, which strongly indicates that $Ag_3PO_4/TiO_2/Fe_3O_4$ nanoparticles are particularly cytotoxic to *E. coli*.[37,38] In addition, a marked enhancement of bactericidal efficiency was observed by combining the photocatalyst with visible-light irradiation. In this case, the *E. coli* cells were completely inactivated. Furthermore, inhibitory concentration tests to quantitatively compare the bactericidal efficiency were carried out. As plotted in Figure S11 (Supporting Information), the presence of 0.15 mg of $Ag_3PO_4/TiO_2/Fe_3O_4$ nanoparticles already showed an obvious suppression of bacterial growth with about 80% inactivation of *E. coli* (10^7 CFU/mL) under visible-light irradiation. The complete suppression of bacterial growth was observed when the $Ag_3PO_4/TiO_2/Fe_3O_4$ loading content was increased to 0.30 mg.

To evaluate the antibacterial activity of the $Ag_3PO_4/TiO_2/Fe_3O_4$ hierarchical nanostructure, the bactericidal efficiency of $Ag_3PO_4/TiO_2/Fe_3O_4$ nanocomposite was compared to the activities of the other photocatalysts. As shown in Figure 5A, a

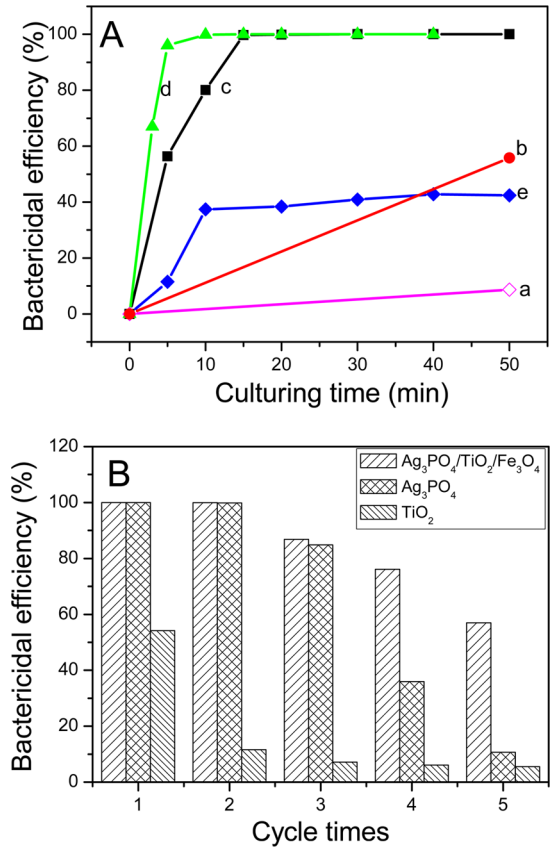

Figure 5. (A) Kinetics of bactericidal efficiency against *E. coli*: (a) *E. coli* suspension without any catalyst irradiated by visible light; (b–d) *E. coli* suspensions with 0.3 mg of (b) TiO_2, (c) Ag_3PO_4, and (d) $Ag_3PO_4/TiO_2/Fe_3O_4$ under visible-light irradiation; (e) *E. coli* suspension with 0.3 mg of $Ag_3PO_4/TiO_2/Fe_3O_4$ incubated in a rotary shaker at 37 °C in the dark. (B) Changes in the bactericidal efficiencies of (a) Ag_3PO_4, (b) Ag_3PO_4/Fe_3O_4, and (c) $Ag_3PO_4/TiO_2/Fe_3O_4$ against *E. coli* (10^7 CFU/mL) under visible-light irradiation for five cycles.

negligible antibacterial activity was observed in the absence of photocatalyst (curve a). Because of the lower photocatalytic activity of TiO_2 under visible light, only 56% inactivation of *E. coli* was found for the TiO_2 sample even after 50 min of irradiation using visible light (curve b). In contrast, marked enhancements in bactericidal efficiency were observed on the Ag_3PO_4- (curve c)

Scheme 1. Preparation and Determination of Bactericidal Activity of Antimicrobial Nanocomposite Films

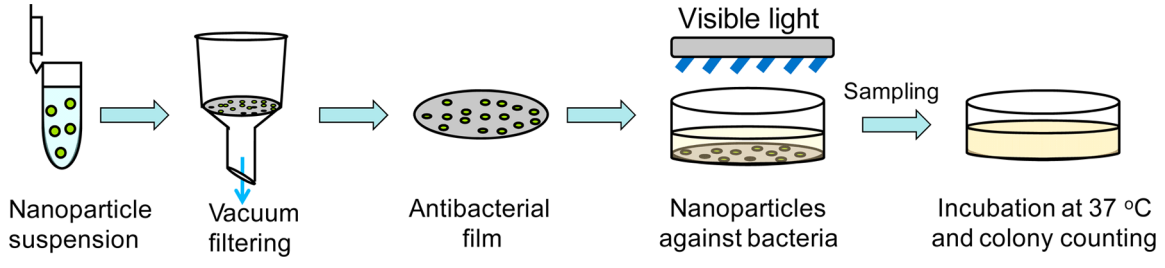

dx.doi.org/10.1021/am5032727 | ACS Appl. Mater. Interfaces 2014, 6, 15122–15131

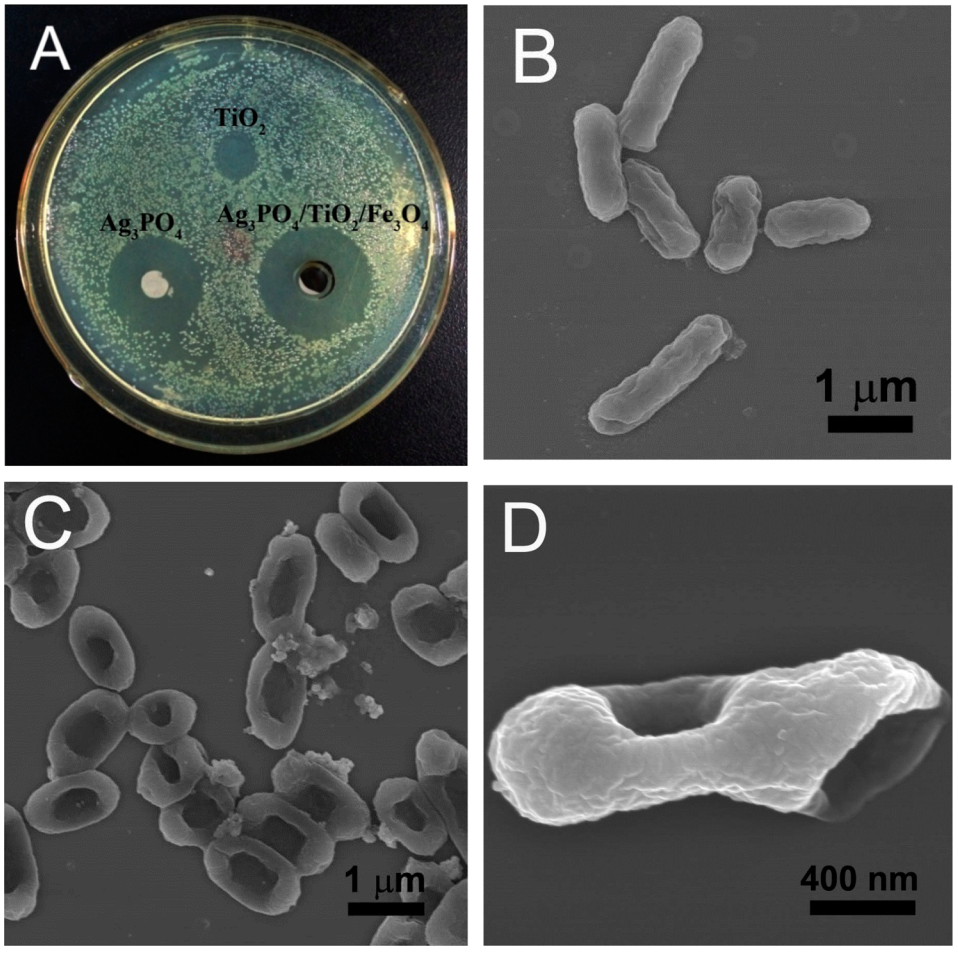

Figure 6. (A) Photographs of antibacterial results on *E. coli* for TiO_2, Fe_3O_4, TiO_2/Fe_3O_4, Ag_3PO_4, Ag_3PO_4/Fe_3O_4, and $Ag_3PO_4/TiO_2/Fe_3O_4$ samples. (B,C) FE-SEM images of *E. coli* (B) before and (C) after being killed on $Ag_3PO_4/TiO_2/Fe_3O_4$ under visible-light irradiation. (D) Enlarged view of a damaged *E. coli* cell.

and $Ag_3PO_4/TiO_2/Fe_3O_4$- (curve d) based antibacterial films upon visible-light illumination. In particular, ~99.8% of the *E. coli* was inactivated on the $Ag_3PO_4/TiO_2/Fe_3O_4$-loaded film only upon irradiation for 5 min (curve d). Additionally, by comparing the bactericidal results on $Ag_3PO_4/TiO_2/Fe_3O_4$-based antibacterial films in the presence (curve d) and absence (curve e) of visible-light irradiation, it is evident that, apart from the effect of the silver ions, a large part of the bactericidal effects is related to the photocatalytic process.[39]

Stability and reusability are also two major challenges in employing photocatalytic materials for antimicrobial applications. To evaluate the antimicrobial stabilities of the as-formed nanocomposites, we further studied the inactivation of Ag_3PO_4-, TiO_2-, and $Ag_3PO_4/TiO_2/Fe_3O_4$-based antibacterial films for several bactericidal cycles. In this study, the as-prepared antibacterial films were reused in five successive antibacterial experiments. The antibacterial films were cleaned by washing with DI water three times before the next photoinactivation of bacteria. As shown in Figure 5B, although some antibacterial activity losses were also observed for the $Ag_3PO_4/TiO_2/Fe_3O_4$ film, the bactericidal efficiency from Ag_3PO_4 films exhibited more significant decreases under the same conditions. Moreover, tests of storage stability revealed that the $Ag_3PO_4/TiO_2/Fe_3O_4$ nanoparticles kept ~97% of their bactericidal activity against *E. coli* after being stored at room temperature for 30 days. Figure S9B (Supporting Information) shows a plot of the silver remaining (measured by centrifuging and dissolving the remaining photocatalyst in HNO_3) after the reuse of the same $Ag_3PO_4/TiO_2/Fe_3O_4$ and Ag_3PO_4 samples for the photoinactivation of *E. coli*. Compared to Ag_3PO_4, the silver concentrations in the $Ag_3PO_4/TiO_2/Fe_3O_4$ nanocomposite decreased much more slowly. This tendency is coincident with the change in bactericidal efficiency in Figure 5B. The results firmly demonstrate that $Ag_3PO_4/TiO_2/Fe_3O_4$-based antibacterial films have satisfied reusability and long-term stability at room temperature.

Qualitative antimicrobial disk diffusion tests were carried out by the Oxford cup method. The *E. coli* (10^7 CFU/mL) was spread on the surface of an LB plate. The as-prepared photocatalyst (0.1 mg) was then filled into an Oxford cup on the LB plate. After exposure to visible light for 5 min, the plate was incubated at 37 °C for 24 h in the dark. As shown in Figure 6A, the Ag_3PO_4 and $Ag_3PO_4/TiO_2/Fe_3O_4$ nanoparticles exhibited clearly visible inhibition zones for *E. coli*, with average diameters of 19 and 24 mm, respectively. The differences in diameter suggest that the $Ag_3PO_4/TiO_2/Fe_3O_4$ nanocomposite had better antimicrobial effects against *E. coli* under visible-light irradiation. The weak antibacterial activities observed for the TiO_2 nanoparticles confirmed that visible light has an insufficient influence on the wide-band-gap photocatalyst. To further understand how the $Ag_3PO_4/TiO_2/Fe_3O_4$ nanocomposite can access and kill *E. coli*, FE-SEM was applied to characterize the

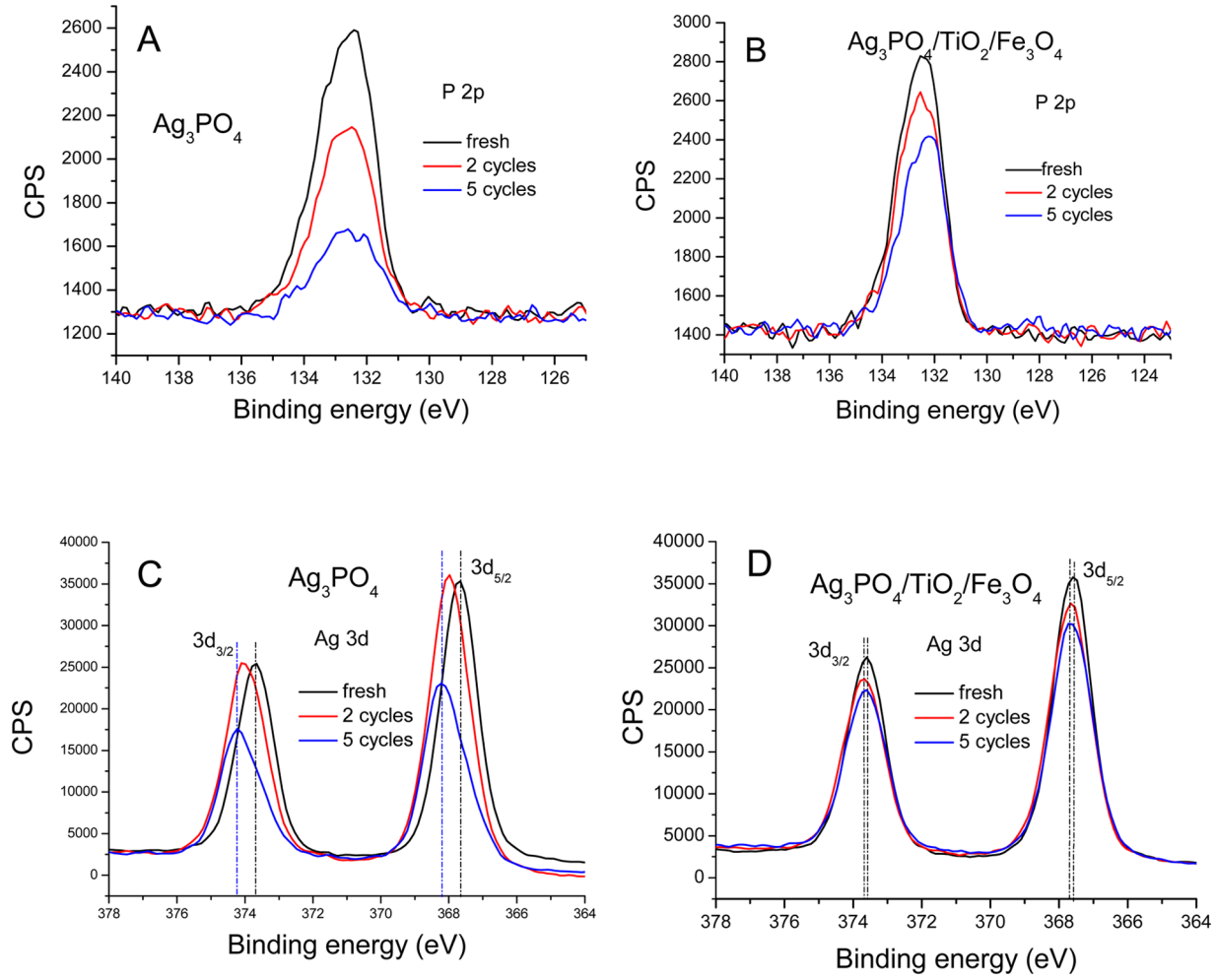

Figure 7. Details of the (A,B) P 2p and (C,D) Ag 3d peaks of the prepared (A,C) Ag_3PO_4 and (B,D) $Ag_3PO_4/TiO_2/Fe_3O_4$ nanoparticles after use in the photocatalytic reaction for 0, 2, and 5 cycles.

bacterial cells before and after the photoinactivation process. As shown in Figure 6B, the intact *E. coli* cells presented a well-defined cell wall. After the damage of *E. coli* on $Ag_3PO_4/TiO_2/Fe_3O_4$ nanocomposite by visible-light irradiation, clear destruction was observed, with the outer membrane collapsed and presented as circles (Figure 6C). As a widely used antibacterial material, silver ions can interact with the main components of the bacterial cell, including the peptidoglycan cell wall and the plasma membrane, cytoplasmic DNA, and bacterial proteins,[16−18] and can also induce collapse of the bacterial membranes[29] during performance of the antibacterial function. In the current study, the $Ag_3PO_4/TiO_2/Fe_3O_4$ nanoparticles were found to anchor closely to the outer walls of the *E. coli* cells. These results are consistent with the phenomena observed by Zeng et al.,[40] who reported that this close-contact configuration could further enhance the photocatalytic activity of the semiconducting composite. A magnified image of *E. coli* is displayed in Figure 6D. Obviously, the outer membrane of the *E. coli* cell is destroyed as well as the ends of the cell after the photoinactivation process.

3.4. Mechanism for the Highly Improved Photocatalytic Antibacterial Activity of $Ag_3PO_4/TiO_2/Fe_3O_4$. The surface components and composition of $Ag_3PO_4/TiO_2/Fe_3O_4$ nanoparticles before and after bactericidal experiments were investigated by XPS analysis. The XPS results in Figure 7 show the main difference in the surface composition of the two different nanoparticles in the P 2p and Ag 3d regions. The P 2p peak of Ag_3PO_4 (Figure 7A) was found to decrease significantly after being reused in two and five successive photocatalytic experiments, which can be attributed to the dissolution of Ag_3PO_4. The P 2p peak of $Ag_3PO_4/TiO_2/Fe_3O_4$ (Figure 7B) exhibited a slight decrease. For the Ag 3d signal, the two broad peaks located at 367.5 and 373.6 eV can be assigned to the doublet Ag $3d_{5/2}$ and Ag $3d_{3/2}$, respectively, of Ag^+ ions.[41] After the photocatalytic reaction, the Ag $3d_{5/2}$ and Ag $3d_{3/2}$ peaks of Ag_3PO_4 showed an obvious decrease and shift to 368.2 and 374.2 eV, respectively. The observed positive shifts can be assigned to the formation of metallic Ag^0. Similar results have been reported by other researchers.[42−44] The Ag $3d_{5/2}$ and Ag $3d_{3/2}$ peaks of $Ag_3PO_4/TiO_2/Fe_3O_4$ also exhibited a slight shift toward higher binding energy as a result of the formation of Ag^0. These results are consistent with the color change observed on Ag_3PO_4 and $Ag_3PO_4/TiO_2/Fe_3O_4$ (after the photocatalytic reaction). The decrements in the P 2p and Ag 3d peak intensities confirm the dissolution of Ag_3PO_4 during the photocatalytic reaction. Moreover, for the $Ag_3PO_4/TiO_2/Fe_3O_4$ nanocomposites, the dissolution of Ag_3PO_4 was slower than that for Ag_3PO_4 itself. Furthermore, the Ag/P atomic concentration ratios for Ag_3PO_4 and $Ag_3PO_4/TiO_2/Fe_3O_4$ nanoparticles after being reused in photocatalytic experiments for 0, 2, and 5 cycles were compared and are plotted in Figure S12 (Supporting Information). Because Ag_3PO_4 can dissolve in aqueous solution during the photo-

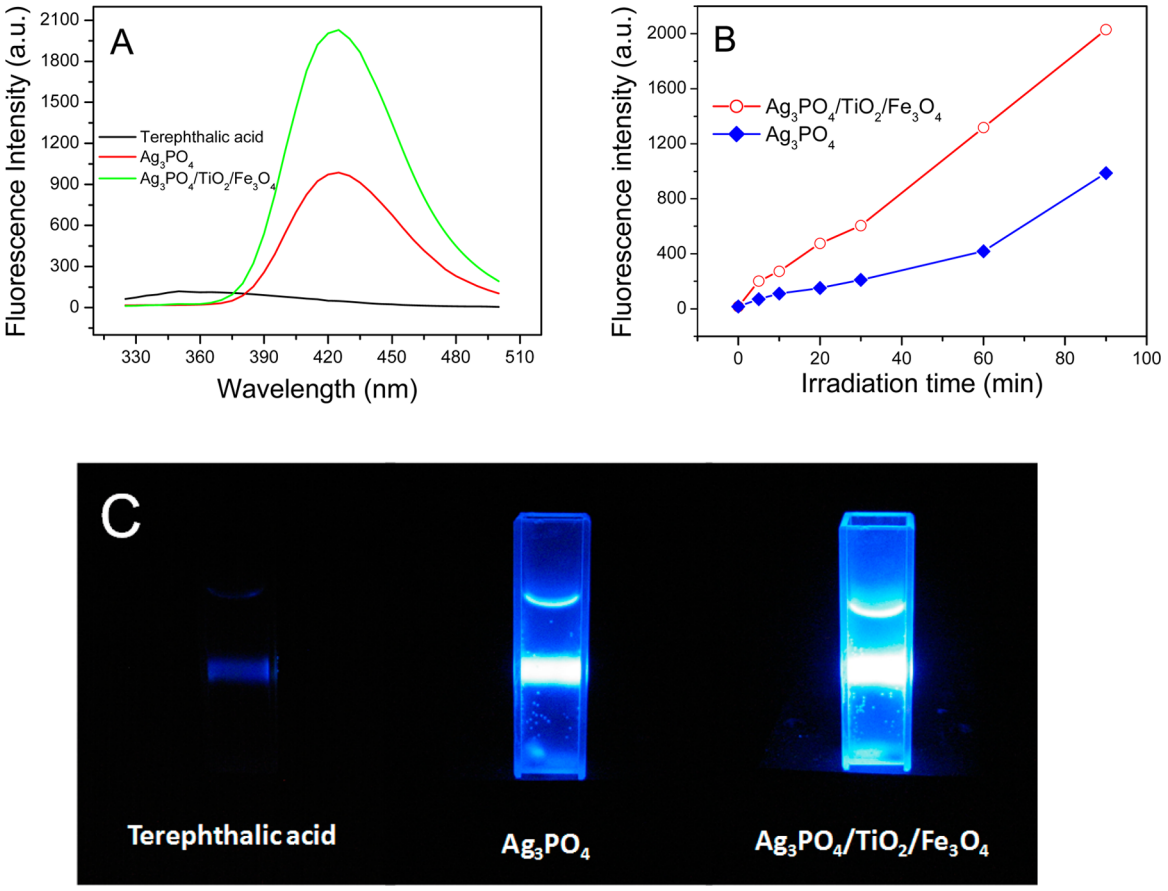

Figure 8. Radical mechanism: (A) Fluorescence spectra obtained for the supernatant liquid of the irradiated Ag_3PO_4 and $Ag_3PO_4/TiO_2/Fe_3O_4$ suspensions containing 3 mM terephthalic acid for 90 min and (B) time dependence of the fluorescence intensity at 426 nm. (C) Fluorescence testing for radical formation by the terephthalic acid reaction for Ag_3PO_4 and $Ag_3PO_4/TiO_2/Fe_3O_4$ before and after visible-light (λ = 405 nm) irradiation for 90 min.

catalysis reaction and Ag^+ ions in solution can be reduced to Ag^0 on the surface of the photocatalyst by the photogenerated electrons, the Ag/P atomic concentration ratio increased with the number of cycles. Compared to $Ag_3PO_4/TiO_2/Fe_3O_4$ nanoparticles, the Ag/P atomic concentration ratio of Ag_3PO_4 nanoparticles increased sharply. Obviously, for $Ag_3PO_4/TiO_2/Fe_3O_4$ nanocomposite, the dissolution of Ag_3PO_4 was slower than that of Ag_3PO_4 itself, which indicates that the $Ag_3PO_4/TiO_2/Fe_3O_4$ nanocomposite was more stable in photocatalytic reaction than the Ag_3PO_4. These results are consistent with the ICP-MS results in Figure S9A (Supporting Information).

To gain more insight into the possible mechanism of the photocatalytic degradation of organic dyes and photoinactivation of bacteria, we performed some additional experiments. It is often perceived that the active oxygen-containing radicals generated in the irradiated system relate to the photoinduced antibacterial activity. To test for $^{\bullet}OH$ radicals, we employed a fluorescence approach based on a terephthalic acid (TA) reaction, which is frequently used in photocatalysis investigations.[44] It is based on the reaction of $^{\bullet}OH$ with TA to form 2-hydroxyterephthalic acid (TAOH) that exhibits a characteristic blue fluorescence at 426 nm. Figure 8A shows the fluorescence response observed for the supernatant solution of Ag_3PO_4 and $Ag_3PO_4/TiO_2/Fe_3O_4$ suspensions containing 3 mM TA irradiated for identical times (90 min). Because the observed fluorescence spectra were identical to that of TAOH, it is concluded that TAOH was generated from TA by the reaction with $^{\bullet}OH$, where $^{\bullet}OH$ was formed during photocatalysis. The fluorescence intensity was plotted (Figure 8B) as a function of the duration of irradiation. Additionally, as exhibited in Figure 8C, a strong blue fluorescence was observed for the solution where $Ag_3PO_4/TiO_2/Fe_3O_4$ nanoparticles were added, and less fluorescence was seen for the Ag_3PO_4 nanoparticles. These results suggest that the $Ag_3PO_4/TiO_2/Fe_3O_4$ hierarchical structure is helpful in producing $^{\bullet}OH$ radicals and favorable for enhanced photocatalytic activity. As mentioned earlier, the antimicrobial activity could not be fully attributed to the dissolved amount of silver ions. In the current work, the photoinduced active oxygen-containing radicals might also impart additional antimicrobial activity.

Herein, the highly enhanced photodegradation and antimicrobial activities achieved on $Ag_3PO_4/TiO_2/Fe_3O_4$ can be assigned to its hierarchical structure. As illustrated in Scheme 2, electron–hole pairs were created within Ag_3PO_4 under the irradiation of visible light, and then the photogenerated holes in Ag_3PO_4 were transferred to the valence band (VB) of TiO_2 and further reacted with the absorbed H_2O molecules to form active oxidants such as hydroxyl radicals ($^{\bullet}OH$). Meanwhile, the photogenerated electrons in the conduction band (CB) migrated to the surface of Ag_3PO_4 and further reacted with absorbed oxygen to form oxidants such as superoxide ions ($^{\bullet}O_2^-$). During the photocatalytic process, Ag^0 nanoparticles were produced by the partial reduction of Ag_3PO_4 by the photogenerated electrons.[45] The resultant Ag metals could trap the photo-

dx.doi.org/10.1021/am5032727 | ACS Appl. Mater. Interfaces 2014, 6, 15122−15131

Scheme 2. Schematic Illustration of Photocatalytic Inactivation toward *E. coli* Using $Ag_3PO_4/TiO_2/Fe_3O_4$ Heterostructure under Visible-Light Irradiation

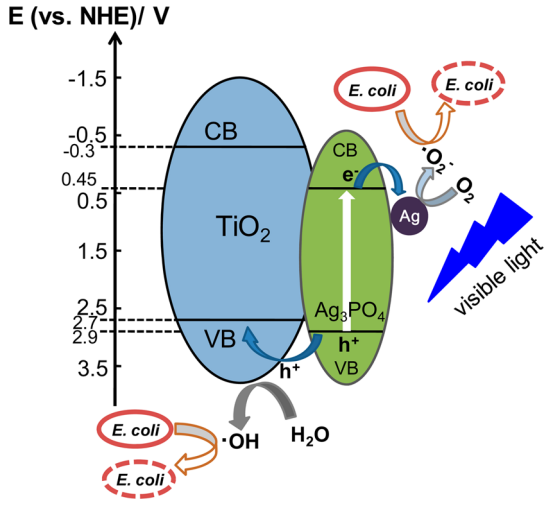

generated electrons and thus inhibit the further decomposition of Ag_3PO_4. Therefore, the formed $Ag/Ag_3PO_4/TiO_2$ interfaces can effectively promote charge separation and enhance the photocatalytic activity of the catalyst. In particular, because the as-prepared $Ag_3PO_4/TiO_2/Fe_3O_4$ nanocomposite exhibits outstanding photocatalytic activity under visible light, the photogenerated reactive oxidants ($^{\bullet}OH$ and $^{\bullet}O_2^-$) oxidize organic compounds/cells adsorbed on the $Ag_3PO_4/TiO_2/Fe_3O_4$ surface and result in the death of the microorganisms. Therefore, the observed breakdown of cell membranes can be attributed to the cytotoxicity of silver ions eluted from the compounds[46−49] and the formation of various reactive oxygen species on photocatalyst/water interfaces under visible-light irradiation.[2,47]

4. CONCLUSIONS

In summary, we have demonstrated in this study that the magnetic $Ag_3PO_4/TiO_2/Fe_3O_4$ nanocomposite is an effective visible-light photocatalysts. The as-prepared $Ag_3PO_4/TiO_2/Fe_3O_4$ nanoparticles can be well-dispersed in water and recovered by an external magnet. Owing to the low band gaps of Ag_3PO_4 and the formed $Ag/Ag_3PO_4/TiO_2$ interface during the photocatalytic reaction, the $Ag_3PO_4/TiO_2/Fe_3O_4$ hierarchical structure exhibited effective charge separation and excellent photocatalytic activity. The photogenerated oxidants ($^{\bullet}OH$ and $^{\bullet}O_2^-$) formed on $Ag_3PO_4/TiO_2/Fe_3O_4$ by visible-light illumination lead to a strong bactericidal effects toward *E. coli*.

■ ASSOCIATED CONTENT

Supporting Information

Some experimental details, TEM and SEM images, XRD measurements, device used for the photocatalytic reaction, influence of catalyst concentration on the photocatalytic degradation, Ag^+ concentration detected by ICP-MS, and effect of visible-light irradiation on the antibacterial activities. This material is available free of charge via the Internet at http://pubs.acs.org.

■ AUTHOR INFORMATION

Corresponding Author

*E-mail: yysong@mail.neu.edu.cn.

Author Contributions

‡These authors contributed equally.

Notes

The authors declare no competing financial interest.

■ ACKNOWLEDGMENTS

This work was supported by the National Natural Science Foundation of China (Nos. 21322504, 21275026, 11174046), the Fundamental Research Funds for the Central Universities (Nos. N120505002, N120505006, N110805001), and the Program for Liaoning Excellent Talents in University (No. LJQ2013028).

■ REFERENCES

(1) Yoshinari, M.; Oda, Y.; Kato, T.; Okuda, K. Influence of Surface Modifications to Titanium on Antibacterial Activity in Vitro. *Biomaterials* **2001**, *22*, 2043−2048.

(2) Etacheri, V.; Michlits, G.; Seery, M. K.; Hinder, S. J.; Pillai, S. C. A Highly Efficient $TiO_{2-x}C_x$ Nano-Heterojunction Photocatalyst for Visible Light Induced Antibacterial Applications. *ACS Appl. Mater. Interfaces* **2013**, *5*, 1663−1672.

(3) Yuvaraj, D.; Kaushik, R.; Rao, K. N. Optical, Field-Emission, and Antimicrobial Properties of ZnO Nanostructured Films Deposited at Room Temperature by Activated Reactive Evaporation. *ACS Appl. Mater. Interfaces* **2010**, *2*, 1019−1024.

(4) Kawashita, M.; Tsuneyama, S.; Miyaji, F.; Kokubo, T.; Kozuka, H.; Yamamoto, K. Antibacterial Silver-Containing Silica Glass Prepared by Sol−Gel Method. *Biomaterials* **2000**, *21*, 393−398.

(5) Fujishima, A.; Honda, K. Electrochemical Photolysis of Water at a Semiconductor Electrode. *Nature* **1972**, *238*, 37−38.

(6) Linsebigler, A. L.; Lu, G.; Yates, J. T. Photocatalysis on TiO_2 Surfaces: Principles, Mechanisms, and Selected Results. *Chem. Rev.* **1995**, *95*, 735−758.

(7) Chen, X.; Shen, S.; Guo, L.; Mao, S. S. Semiconductor-Based Photocatalytic Hydrogen Generation. *Chem. Rev.* **2010**, *110*, 6503−6570.

(8) Asahi, R.; Morikawa, T.; Ohwaki, T.; Aoki, K.; Taga, Y. Visible-Light Photocatalysis in Nitrogen-Doped Titanium Oxides. *Science* **2001**, *293*, 269−271.

(9) Roy, P.; Dey, T.; Lee, K.; Kim, D.; Fabry, B.; Schmuki, P. Size-Selective Separation of Macromolecules by Nanochannel Titania Membrane with Self-Cleaning (Declogging) Ability. *J. Am. Chem. Soc.* **2010**, *132*, 7893−7895.

(10) Song, Y.-Y.; Schmidt-Stein, F.; Bauer, S.; Schmuki, P. Amphiphilic TiO_2 Nanotube Arrays: An Actively Controllable Drug Delivery System. *J. Am. Chem. Soc.* **2009**, *131*, 4230−4232.

(11) Applerot, G.; Lipovsky, A.; Dror, R.; Perkas, N.; Nitzan, Y.; Lubart, R.; Gedanken, A. Enhanced Antibacterial Activity of Nanocrystalline ZnO Due to Increased ROS-Mediated Cell Injury. *Adv. Funct. Mater.* **2009**, *19*, 842−852.

(12) Gerischer, H.; Heller, A. The Role of Oxygen in Photooxidation of Organic Molecules on Semiconductor Particles. *J. Phys. Chem.* **1991**, *95*, 5261−5267.

(13) Yi, Z.; Ye, J.; Kikugawa, N.; Kako, T.; Ouyang, S.; Williams, H. S.; Yang, H.; Cao, J.; Luo, W.; Li, Z. An Orthophosphate Semiconductor with Photooxidation Properties under Visible-Light Irradiation. *Nat. Mater.* **2010**, *9*, 559−564.

(14) Wu, A.; Tian, C.; Chang, W.; Hong, Y.; Zhang, Q.; Qu, Y.; Fu, H. Morphology-Controlled Synthesis of Ag_3PO_4 Nano/Microcrystals and Their Antibacterial Properties. *Mater. Res. Bull.* **2013**, *48*, 3043−3048.

(15) Liu, J. K.; Luo, C. X.; Wang, J. D.; Yang, X. H.; Zhong, X. H. Controlled Synthesis of Silver Phosphate Crystals with High Photocatalytic Activity and Bacteriostatic Activity. *CrystEngComm* **2012**, *14*, 8714−8721.

(16) Zhao, G. J.; Stevens, S. E. Multiple Parameters for the Comprehensive Evaluation of the Susceptibility of *Escherichia coli* to the Silver Ion. *Biomaterials* **1998**, *11*, 27−32.

(17) Yamanaka, M.; Hara, K.; Kudo, J. Bactericidal Actions of a Silver Ion Solution on *Escherichia coli*, Studied by Energy-Filtering Transmission Electron Microscopy and Proteomic Analysis. *Appl. Environ. Microbiol.* **2005**, *71*, 7589−7593.
(18) Jung, W. K.; Koo, H. C.; Kim, K. W.; Shin, S.; Kim, S. H.; Park, Y. H. Antibacterial Activity and Mechanism of Action of the Silver Ion in *Staphylococcus aureus* and *Escherichia coli*. *Appl. Environ. Microbiol.* **2008**, *74*, 2171−2178.
(19) Yang, W. J.; Shen, C. C.; Ji, Q. L.; An, H. J.; Wang, J. J.; Liu, Q. D.; Zhang, Z. Z. Food Storage Material Silver Nanoparticles Interfere with DNA Replication Fidelity and Bind with DNA. *Nanotechnology* **2009**, *20*, 085102.
(20) Shrivastava, S.; Bera, T.; Roy, A.; Singh, G.; Ramachandrarao, P.; Dash, D. Characterization of Enhanced Antibacterial Effects of Novel Silver Nanoparticles. *Nanotechnology* **2007**, *18*, 225103.
(21) Liu, Y.; Wang, X.; Yang, F.; Yang, X. Excellent Antimicrobial Properties of Mesoporous Anatase TiO_2 and Ag/TiO_2 Composite Films. *Microporous Mesoporous Mater.* **2008**, *114*, 431−439.
(22) Yao, W.; Zhang, B.; Huang, C.; Ma, C.; Song, X.; Xu, Q. Synthesis and Characterization of High Efficiency and Stable Ag_3PO_4/TiO_2 Visible Light Photocatalyst for the Degradation of Methylene Blue and Rhodamine B Solutions. *J. Mater. Chem.* **2012**, *22*, 4050−4055.
(23) Bi, Y.; Ouyang, S.; Umezawa, N.; Cao, J.; Ye, J. Facet Effect of Single-Crystalline Ag_3PO_4 Sub-Microcrystals on Photocatalytic Properties. *J. Am. Chem. Soc.* **2011**, *133*, 6490−6492.
(24) Rawal, S. B.; Sung, S. D.; Lee, W. I. Novel Ag_3PO_4/TiO_2 Composites for Efficient Decomposition of Gaseous 2-Propanol under Visible-Light Irradiation. *Catal. Commun.* **2012**, *17*, 131−135.
(25) Teng, W.; Li, X.; Zhao, Q.; Chen, G. Fabrication of $Ag/Ag_3PO_4/TiO_2$ Heterostructure Photoelectrodes for Efficient Decomposition of 2-Chlorophenol under Visible Light Irradiation. *J. Mater. Chem. A* **2013**, *1*, 9060−9068.
(26) Hu, H.; Jiao, Z.; Yu, H.; Lu, G.; Ye, J.; Bi, Y. Facile Synthesis of Tetrahedral Ag_3PO_4 Submicro-Crystals with Enhanced Photocatalytic Properties. *J. Mater. Chem. A* **2013**, *1*, 2387−2390.
(27) Dinh, C. T.; Nguyen, T. D.; Kleitz, F.; Do, T. O. Large-Scale Synthesis of Uniform Silver Orthophosphate Colloidal Nanocrystals Exhibiting High Visible Light Photocatalytic Activity. *Chem. Commun.* **2011**, *47*, 7797−7799.
(28) Bi, Y.; Hu, H.; Ouyang, S.; Jiao, Z.; Lu, G.; Ye, J. Selective Growth of Metallic Ag Nanocrystals on Ag_3PO_4 Submicro-Cubes for Photocatalytic Applications. *Chem.−Eur. J.* **2012**, *18*, 14272−14275.
(29) Teng, W.; Li, X.; Zhao, Q.; Zhao, J.; Zhang, A. In Situ Capture of Active Species and Oxidation Mechanism of RhB and MB Dyes Over Sunlight-Driven Ag/Ag_3PO_4 Plasmonic Nanocatalyst. *Appl. Catal. B: Environ.* **2012**, *125*, 538−545.
(30) Yang, X.; Qin, J.; Jiang, Y.; Li, R.; Li, Y.; Tang, H. Bifunctional TiO_2/Ag_3PO_4/Graphene Composites with Superior Visible Light Photocatalytic Performance and Synergistic Inactivation of Bacteria. *RSC Adv.* **2014**, *4*, 18627−18636.
(31) Li, G.; Mao, L. Magnetically Separable Fe_3O_4-Ag_3PO_4 Sub-Micrometre Composite: Facile Synthesis, High Visible Light-Driven Photocatalytic Efficiency, and Good Recyclability. *RSC Adv.* **2012**, *2*, 5108−5111.
(32) Guo, X.; Chen, N.; Feng, C.; Yang, Y.; Zhange, B.; Wang, G.; Zhang, Z. Performance of Magnetically Recoverable Core−Shell Fe_3O_4@Ag_3PO_4/AgCl for Photocatalytic Removal of Methylene Blue under Simulated Solar Light. *Catal. Commun.* **2013**, *38*, 26−30.
(33) Wang, P.; Huang, B.; Lou, Z.; Zhang, X.; Qin, X.; Dai, Y.; Zheng, Z.; Wang, X. Synthesis of Highly Efficient Ag@AgCl Plasmonic Photocatalysts with Various Structures. *Chem.—Eur. J.* **2010**, *16*, 538−544.
(34) Lorenz, K.; Bauer, S.; Gutbrod, K.; Guggenbichler, J. P.; Schmuki, P.; Zollfrank, C. Anodic TiO_2 Nanotube Layers Electrochemically Filled with MoO_3 and Their Antimicrobial Properties. *Biointerphases* **2011**, *6*, 16−21.
(35) Kamat, P. V. Photochemistry on Nonreactive and Reactive (Semiconductor) Surfaces. *Chem. Rev.* **1993**, *93*, 267−300.
(36) Bi, Y.; Hu, H.; Ouyang, S.; Jiao, Z.; Lu, G.; Ye, J. Selective Growth of Ag_3PO_4 Submicro-Cubes on Ag Nanowires to Fabricate Necklace-Like Heterostructures for Photocatalytic Applications. *J. Mater. Chem.* **2012**, *22*, 14847−14850.
(37) Bates, C. W.; Wertheim, G. K.; Buchanan, D. N. E. Nature of the 3.8 eV Plasmon in X-ray Photoemission from Silver. *Phys. Lett. A* **1979**, *72*, 178−180.
(38) Wang, P.; Huang, B.; Zhang, Q.; Zhang, X.; Qin, X.; Dai, Y.; Zhan, J.; Yu, J.; Liu, H.; Lou, Z. Highly Efficient Visible Light Plasmonic Photocatalyst Ag@Ag(Br, I). *Chem.—Eur. J.* **2010**, *16*, 10042−10047.
(39) Lv, M.; Su, S.; He, Y.; Huang, Q.; Hu, W.; Li, D.; Fan, C.; Lee, S.-T. Long-Term Antimicrobial Effect of Silicon Nanowires Decorated with Silver Nanoparticles. *Adv. Mater.* **2010**, *22*, 5463−5467.
(40) Pang, M.; Hu, J.; Zeng, H. C. Synthesis, Morphological Control, and Antibacterial Properties of Hollow/Solid Ag_2S/Ag Heterodimers. *J. Am. Chem. Soc.* **2010**, *132*, 10771−10785.
(41) Liu, R.; Hu, P.; Chen, S. Photocatalytic Activity of Ag_3PO_4 Nanoparticle/TiO_2 Nanobelt Heterostructures. *Appl. Surf. Sci.* **2012**, *258*, 9805−9809.
(42) Fujishima, A.; Zhang, X. T.; Tryk, D. A. TiO_2 Photocatalysis and Related Surface Phenomena. *Surf. Sci. Rep.* **2008**, *63*, 515−582.
(43) Ren, N.; Li, R.; Chen, L.; Wang, G.; Liu, D.; Wang, Y.; Zheng, L.; Tang, W.; Yu, X.; Jiang, H.; Jiang, H.; Liu, H.; Wu, N. In-Situ Construction of Titanate−Silver Nanoparticle−Titanate Sandwich Nanostructure on Metallic Titanium Surface for Bacteriostatic and Biocompatible Implants. *J. Mater. Chem.* **2012**, *22*, 19151−19160.
(44) Song, Y.-Y.; Roy, P.; Paramasivam, I.; Schmuki, P. Voltage-Induced Payload Release and Wettability Control on TiO_2 and TiO_2 Nanotubes. *Angew. Chem., Int. Ed.* **2010**, *49*, 351−354.
(45) Wang, P.; Huang, B.; Qin, X.; Zhang, X.; Dai, Y.; Whangbo, M. H. $Ag/AgBr/WO_3{\cdot}H_2O$: Visible-Light Photocatalyst for Bacteria Destruction. *Inorg. Chem.* **2009**, *48*, 10697−10702.
(46) Wu, X.; Li, J.; Wang, L.; Huang, D.; Zuo, Y.; Li, Y. The Release Properties of Silver Ions from Ag−*n*HA/TiO_2/PA66 Antimicrobial Composite Scaffolds. *Biomed. Mater.* **2010**, *5*, 044105.
(47) Song, Y. Y.; Yang, T.; Cao, J.; Gao, Z. D.; Lynch, R. P. Protein-Mediated Synthesis of Antibacterial Silver Nanoparticles Deposited on Titanium Dioxide Nanotube Arrays. *Microchim. Acta* **2012**, *177*, 129−135.
(48) Hwang, E. T.; Lee, J. H.; Chae, Y. J.; Kim, Y. S.; Kim, B. C.; Sang, B. I.; Gu, M. B. Analysis of the Toxic Mode of Action of Silver Nanoparticles Using Stress-Specific Bioluminescent Bacteria. *Small* **2008**, *4*, 746−750.
(49) Wang, Q. F.; Yu, H. J.; Zhong, L.; Liu, J. Q.; Sun, J. Q.; Shen, J. C. Incorporation of Silver Ions into Ultrathin Titanium Phosphate Films: In Situ Reduction to Prepare Silver Nanoparticles and Their Antibacterial Activity. *Chem. Mater.* **2006**, *18*, 1988−1994.